Brain tumour segmentation from MRI using superpixels based spectral clustering

M. Angulakshmi, G.G. Lakshmi Priya

PII: S1319-1578(17)30347-6
DOI: https://doi.org/10.1016/j.jksuci.2018.01.009
Reference: JKSUCI 401

To appear in: *Journal of King Saud University - Computer and Information Sciences*

Received Date: 25 October 2017
Revised Date: 29 December 2017
Accepted Date: 30 January 2018

Please cite this article as: Angulakshmi, M., Lakshmi Priya, G.G., Brain tumour segmentation from MRI using superpixels based spectral clustering, *Journal of King Saud University - Computer and Information Sciences* (2018), doi: https://doi.org/10.1016/j.jksuci.2018.01.009

Brain tumour segmentation from MRI using superpixels based spectral clustering

ANGULAKSHMI. M[1]. LAKSHMI PRIYA.G.G[2]

[1] VIT University, Vellore, Tamil Nadu, India.

[2*] VIT University, Vellore, Tamil Nadu, India.

[1] angulakshmi.m@vit.ac.in, [2*]lakshmipriya.gg@vit.ac.in

Brain tumour segmentation from MRI using superpixels based spectral clustering

Abstract

The automated brain tumour segmentation method is becoming challenging in the field of medical research as a brain tumour emerges with diverse size, shape and intensity. In this paper, spectral clustering is used for segmentation of brain tumour tissues from Magnetic resonance images (MRI) as it creates high-quality clusters. Spectral clustering suffers from dense similarity matrix construction for massive data. To overwhelm the drawback of spectral clustering, the proposed method performs the brain tumour segmentation by (i) identifying the tumorous region labelled as Region of Interest (ROI) using superpixel based spectral clustering. (ii) brain tumour tissues are then segmented by performing spectral clustering over the obtained ROI of MRI. The identification of ROI alleviates the computational burden of spectral clustering. The segmentation of ROI using spectral clustering produces high-quality clustering results for brain tumour segmentation. The observational results are taken out on BRATS 2012 dataset and evaluated using dice score, sensitivity and specificity metrics. The proposed method outperforms the other clustering methods with competitive dice score values for segmentation of edema and Tumor Core (TC) regions from MRI images.

Keywords: Brain tumour, Region of Interest, Segmentation, Superpixels, Spectral clustering, MRI

1. Introduction

A brain tumour is an uncontrolled growth of cells in the brain (Gordillo et al., 2013). The death of people due to a brain tumour is increasing in last few decades. A tumour can be classified as the malignant or benign. A cyst with no cancer cells is called as benign. They can be deleted entirely and do not reproduce after their removal. Benign tumours are less aggressive and do not intrude on the nearby tissues. A tumour with cancer cells is called as malignant, which is more aggressive and they rise rapidly with increasing pressure in the head. They invade the nearby tissues in the brainand other parts of the body, such as spinal cord beyond where it has grown. Magnetic Resonance Imaging (MRI) technique is widely applied in the medical field due to its high spatial resolution, soft tissue contrast and non-invasive characteristics. MRI provides rich information for brain tumour diagnosis and treatment planning (Bauer et al., 2013). As a brain tumour varies in shape, size and intensity, makes tumour segmentation process more tedious. The four slices of MRI are T1, T2, T1 contrast and FLAIR images (shown in Fig.1) are used for the extraction of brain tumours. The blood barrier disruption is acquired from T1 weighted imaging with contrast enhancement. The necrotic area can be observed by hypo-intense part of the Tumor Core (TC) in the T1contrast image. The T2-weighted (T2) and the Fluid-Attenuated Inversion Recovery (FLAIR) MRI are utilised for finding the extension of a tumour and edema (Yuhong, 2016). Nevertheless, MRI images are also affected by intensity inhomogeneity (Xiaofei, 2015) and weak radio frequency (GeethuMohan and MonicaSubashini, 2018) that might affect the accuracy of segmentation technique. The brain tumour segmentation is a process of identifying affected tumour tissues and protects healthy tissues from damage by destroying identified tumour tissues in the brain. In clinical practice, this undertaking of identifying tumour tissues is performed with manual annotations. As the manual process is a time-consuming process, development of automatic segmentation becomes exciting and vital research domain in recent years (Angulakshmi and Lakshmipriya, 2017).

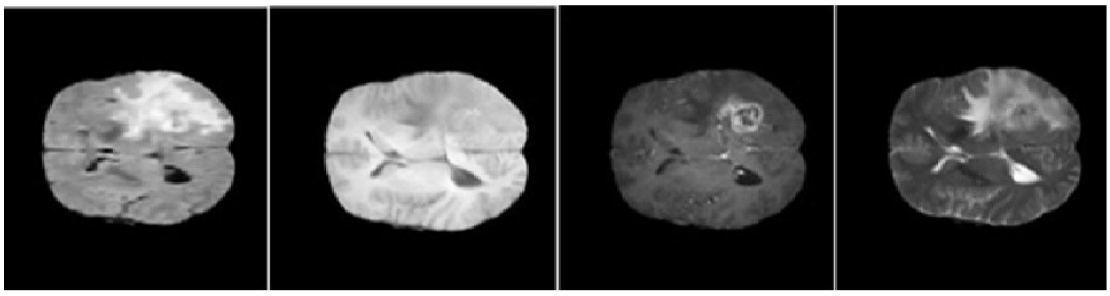

Fig. 1 a. FLAIR image b. T1 image c. T1 contrast image d. T2 image

In general, the automatic brain tumour segmentation methods are classified as supervised and unsupervised segmentation techniques (Gordillo et al., 2013). The supervised method demands massive datasets with the valid ground truth. Whereas, gathering labelled dataset manually is challenging and time-consuming task. On the other hand, unsupervised method does not depend on any training dataset and can be applied to the dataset of different imaging protocols. We have investigated that unsupervised clustering methods can be used to reduce complexity and to promote execution speed without loss of accuracy for segmentation. As spectral clustering obtains an optimal global solution among other clustering techniques, we focus on spectral clustering for segmentation of a brain tumour. The spectral clustering performs grouping of data (clusters) using the graph Laplacian of the data. Eigenvectors and Eigenvalues of the Laplacian matrix furnish the vital information of the connected components of the given data. The set of Eigenvalues of Laplacian matrix is called as "Spectrum" of the graph. So it gains the name "Spectral Clustering". The primary limitation of Spectral clustering is dense affinity matrix construction for eigen decomposition (Donghui et al., 2009).

In this paper, the ROI based segmentation using spectral clustering is proposed for brain tumour segmentation. To segment tumour tissues from the MRI images, the spectral grouping of superpixels is performed to identify the tumorous region (ROI) in the image. The superpixels are generated by estimating the central tendency value (mean or median or mode value) of the equal sized blocks of the image. These superpixels incorporate local neighbourhood spatial information in the clustering task to increase the noise immunity. The size of the image is scaled down to the tumorous region, labelled as ROI for segmentation. Finally, ROI is segmented by spectral clustering method to produce the high-quality clustering accuracy for segmenting brain tumour tissues. Fig. 2. shows the flow diagram of the proposed work. The rest of the paper is organised as follows. Related works are discussed in Section 2. Basic concepts are overviewed in Section 3. The proposed method is presented in section 4. Experimental results and discussions are carried into section 5, and finally, the conclusion is discussed in section 6.

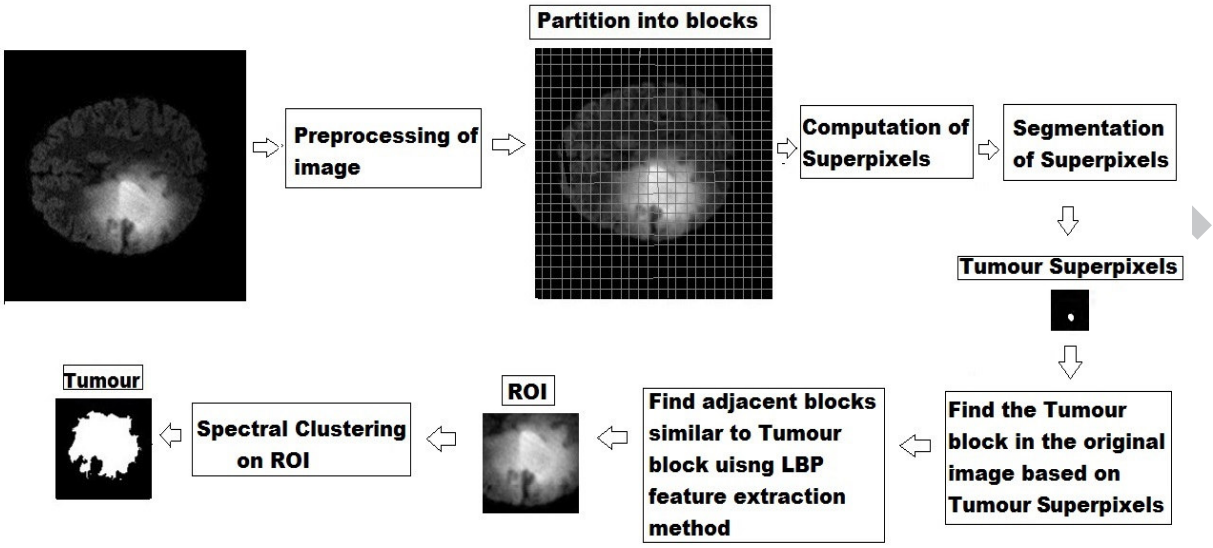

Fig. 2. Flow diagram of proposed work

2. Related works

As this paper focuses on unsupervised method, few related unsupervised techniques are discussed in this section. Unsupervised methods for performing brain tumour segmentation include Graph Cut (Corso et al., 2008), Fuzzy-C-Means (FCM) (Emblem et al., 2009), Gaussian Mixture Model (GMM) (Liang et al. 2012), and K-means (Tuhin et al., 2012). In the paper (Phillips et al., 1995), the authors have used initially the fuzzy technique for brain tumour segmentation. Later, it was combined with the knowledge-based methods for more reliable performance (Emblem et al., 2009). The clustering scheme utilises the pixels of the image to produce clusters algorithmically. The FCM method is likewise blended with other techniques to provide better segmentation results (Zexuan et al., 2012; Yogita et al., 2016; AnithaVishnuvarthanan et al. 2017).

The K-means clustering is another popularly used clustering technique for brain tumour segmentation (Tuhin et al., 2012; Madhukumar and Santhiyakumari, 2015). The K- means algorithm suffers from initial seed point selection during clustering task and thus non-deterministic. The GMM is often employed for modelling unsupervised brain tumour segmentation method (Liang et al. 2012; Menze et al., 2015). The GMM works by finding the maximum likelihood parameter of the Gaussian mixture for fitting the input information. The Expected maximization (EM) is applied for solving the optimization problem in GMM. In the paper (Juan-Albarracín et al., 2015), the GMM is used to produce competitive results with state of the art unsupervised algorithms for brain tissue segmentation. The conventional unsupervised clustering algorithms include local information into the clustering task. The local spatial data of each pixel is taken to involve values, as the mean or median of the neighbours, within a specified window around it. In the paper (Sauwen et al., 2016), the authors have addressed the conventional FCM, K means, and GMM as the non-convex methods as they produce the optimal local solution. Recently, many researchers (Jeetashree et al., 2016) have incorporated the spatial information into the conventional clustering algorithms to improve the performance of image segmentation.

In the last few years, graph cut is also popularly used method for image segmentation (Corso et al., 2008), as it produces the globally optimal solution. The spectral clustering is one of the graph-cut based clustering methods (Jianbo and Jitendra, 2000; Andrew et al., 2001). The method is successful because it can produce an approximately global optimal solution in polynomial time. Spectral clustering makes no assumption about the shape of the cluster or the density distribution of data points. The intertwined spiral can also be generated using spectral clustering. However, graph cut-based method often needs to work out a generalized eigenvector problem and may tolerate from the heavy computational load when the data set is massive.

To overcome the drawback of spectral clustering, Nystrom method performs the Low-rank approximation of large affinity matrix (Fowlkes et al., 2004). The technique produces better segmentation accuracy. Nevertheless, the accuracy of segmentation result is affected, due to the heavy dataset and the non-orthogonal eigenvectors. In the fast approximate spectral clustering (Donghui et al., 2009) method, the clustering on the set of representative points is performed on the original image. According to this method, the pixels are clustered into k groups using the K - means algorithm in the preprocessing stage. Only the centroids of k clusters are considered for further segmentation using spectral clustering. However, the geometrical structures were not efficiently captured by representative data points**.**

The superpixel was initially suggested by (Xiaofeng and Jitendra, 2003) represents a coherent local region that keeps most of the features necessary for image mining. The estimation of the superpixels can dramatically shorten the number of nodes in the graph and speed up the graph partition while maintaining the image data. The superpixels also incorporate local spatial data for clustering to increase noise immunity. The brain tumour segmentation is also performed successfully using spectral clustering (Yang and Grigsby, 2010; Padole and Chaudhari, 2012). In the paper (Po et al., 2013) have generated superpixels using K-means clustering followed by segmentation of superpixels by spectral clustering for brain tumour segmentation. Motivated by the successful application of spectral clustering and superpixels in the segmentation process, we have proposed spectral clustering of superpixels for ROI based segmentation of brain tumours. The main contributions of this paper are summarized as follows

- A new method is suggested to reduce down the size of MRI brain tumour image to ROI (tumorous region) using superpixels. The ROI extraction reduces the dense similarity matrix formation of spectral clustering.
- The segmentation of ROI using spectral clustering finds a global anatomical relationship between pixels to develop the high quality global optimal solution for brain tumour segmentation.

The proposed method can also be used for indexing the large brain tumour database. The indexing also helps the physician to retrieve large images for diagnosis and treatment planning of tumour disease.

3. Basic Concepts

In this section, description about Non-Local Mean (NLM) filter and spectral clustering are specified.

3.1 Non Local Mean Filter

The denoising methods deal with the removal of noises from MRI images. The Non-Local Mean (NLM) filtering technique by (Buades et al. 2005), is found to function well with Gaussian and Rician distribution of noise in MRI images. No assumption is made on the location of the pixel for filtering a pixel of interest. The NLM filter utilized the advantage of the high degree of redundancy in the image. The NLM filter works by restoring all pixels in the given image with a weighted average of neighbouring pixel value using similarity measures. Let discrete grid of pixels is represented by G. For the given image $u = \{u_i\}$, where $i \in G$, the restored weight of a pixel i is calculated using the weighted average of all pixel of the image u. It is denoted as $NLM(u_i)$ and calculated using the Eq (1)

$$NLM(u_i) = \sum_{j=G} w(i,j) u_j \tag{1}$$

G denotes discrete grid of pixels. The symbol u_j is original the intensity at the pixel j. Where $w(i,j)$ is the weight allotted to u_j in intensity restoration at the pixel i. It depends on the similarity between pixels i and j. It also satisfies the condition $0 \le w(i,j) \le 1$ and $\sum_{j=G} w(i,j) = 1$

The weights are defined as follows in Eq (2).

$$w(i,j) = \frac{1}{Z(i)} \exp\left(-\frac{\left\| u(L_i) - u(L_j) \right\|_{2,a}^2}{h^2}\right) \tag{2}$$

where $Z(i)$ stands for normalizing factor and h stands for degree of filtering or smoothening factor. Let the two similarity patch windows, centered at the pixel i and pixel j is given by the term L_i *and* L_j respectively. The term $u(L_i)$ represents the vector of adjacent image intensity squared neighbourhood in patch window L_i. The term $u(L_j)$ represents the vector of adjacent image intensity squared neighbourhood in patch window L_j. The similarity is evaluated with the aid of the decreasing function of the weighted Euclidian distance and denoted as ($\|\cdot\|_{2,a}^2$) and shown in the Eq (3) to measure the similarity between two patch windows L_i *and* L_j.

$$\left\| (u(L_i) - u(L_j) \right\|_{2,a}^2 \tag{3}$$

Where a denotes the standard deviation of the Gaussian kernel. The similar pixels have larger weights on average.

3.2 Spectral Clustering

One of the popular unsupervised clustering techniques based on the graph is spectral clustering (Jianbo and Jitendra, 2000; Andrew et al., 2001). The spectral clustering performs grouping of data (clusters) by decomposing eigenvectors and eigenvalues of Laplacian matrix. The vital data of the connected components of the passed information is furnished by the eigenvectors and eigenvalues

of the Laplacian matrix. Given an image $I = \{I_1, I_2 ... I_n\} \notin R^d$, where $I_1, I_2 .. I_n$ denotes pixels in the image. The image is represented as a weighted graph $G = \{V, E\}$ where V represents set of nodes in the graph and E denote the relationship between nodes. The graph is represented as similarity matrix S where i^{th} and j^{th} row of similarity matrix is given by the equation Eq (4)

$$S_{ij} = \begin{Bmatrix} e^{-\frac{d(I_i, I_j)^2}{2\sigma^2}} & , i \neq j \\ 0 & , i = j \end{Bmatrix}, \quad (4)$$

where $d(I_i, I_j)$ denotes the Euclidian distance between node $I_i and I_j$. The symbol σ =1 for the weighted graph that controls the level of the intensity of the neighborhood. Later similarity matrix is converted to a normalized Laplacian matrix for eigenvector decomposition. Finally, the largest k eigenvectors are clustered using the K-means algorithm to get clusters of original information.

4. The Proposed method

In the proposed method, the ROI that contains information of tumorous tissue is segmented using spectral clustering rather than considering the whole image. The data reduction is performed using superpixels. The superpixels are generated using the Central Tendency Value (CTV) of blocks of the image. These superpixels are considered as nodes for spectral clustering to identify ROI. As the result of segmentation of superpixels, tumor superpixel and non-tumour superpixels are obtained. The original block of tumour superpixel in the image is denoted as tumour block. The adjacent blocks similar to the tumour block are extracted using Local Binary Pattern (LBP) feature extraction techniques to form ROI. Lastly, the ROI is segmented using spectral clustering to represent various tumour tissues. The proposed method is explained in the following sections.

4.1 Preprocessing

The preprocessing step is performed to make the images suitable for processing in Computer Aided Design (CAD) system by suppressing unwanted distortions or enhancing some image features important. As unsupervised segmentation has no references or manual labelled model, artifacts such noise and intensity inhomogeneity are high during the processing of images. Due to this factor, the results of clustering may be affected during segmentation. To reduce the impact of unwanted distortion, pre-processing techniques that involve NLM filtering (Buades et al. 2005) method and N4ITK Bias field correction (Tustison et al. 2010) are performed for images in the proposed method. In the proposed study, bias correction is applied to T1c image modularity. After pre-processing the image, ROI identification is carried out. The explanation for ROI identification is employed in the succeeding section.

4.2. Region of Interest (ROI) Identification

The size of the image is scaled down to ROI which is smaller than the original image. The ROI in the proposed method represents an abnormal region, which holds in a tumour. Due to ROI identification, the non-tumours part in the given image is removed for tumour segmentation. Only the essential tumorous region is examined for further processing. The spectral clustering is then performed on ROI, and the dense similarity matrix construction for spectral clustering is reduced

with no loss in the high quality of spectral clustering accuracy. The process of ROI identified has the following steps and explained in following subsections.

- Computation of superpixels
- Segmentation of superpixels.
- Identification of tumour block.
- Identification of adjacent blocks

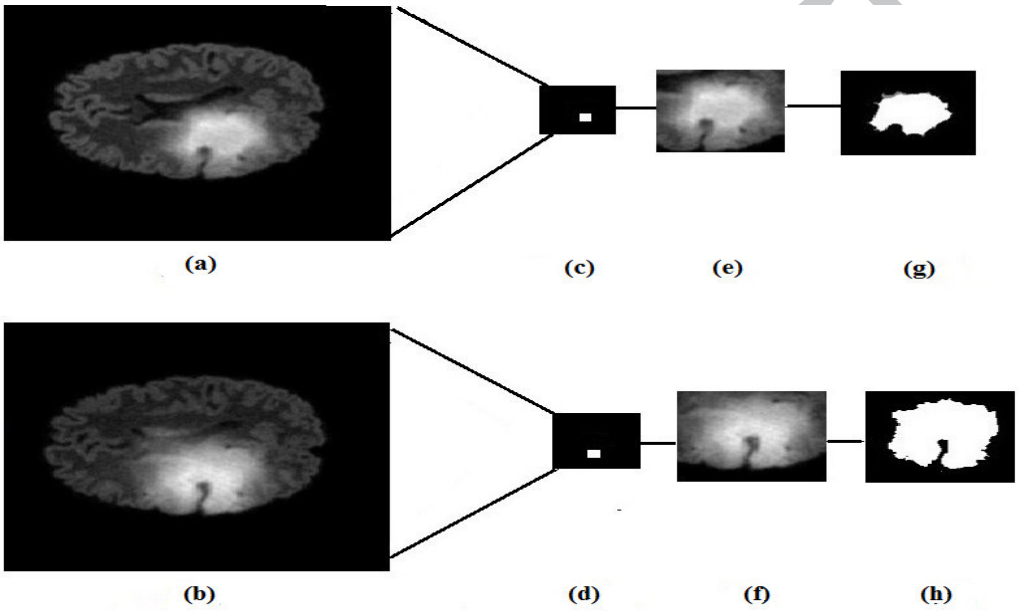

Fig. 3. Segmentation result of the proposed method for two patient images(a) and (b). (a)-(b): T1 contrast brain tumour image. (c)-(d): Segmentation results of superpixels. (e)-(f) : ROI. (g)-(h): TC

4.2.1. Computation of superpixels.

In the proposed method, the image is partitioned into small equal sized blocks. The Central Tendency Value (CTV) usually denotes the tendency of data to organize the group around some key value. In the proposed method, the CTV of each block is calculated using mean, median, mode and used as the superpixel value of the corresponding block. The mean value of a block is estimated by taking the mean of all pixel values in a block. .

Let $B_1, B_2..B_m$ represents the blocks of the image I , where m denotes the number of the blocks. Let us consider the pixel intensity values as $P^1, P^2..P^n$, where n represents the number of pixels in a block. CTV computed using mean M_i represents the mean value of the i^{th} block B_i and given in Eq. 5.

$$M_i = \frac{1}{n}\sum_{j=1}^{n} P_j^i \quad (5)$$

Where $i = 1,2...m, no\ of\ blocks$ of the image I. P_j^i is $the\ j^{th}$ pixel value of i^{th} the block B_i in the given image I. Where $j = 1,2...n, no\ of\ pixels\ in\ i^{th}\ block$ of the image I.

CTV computed using median Med_i represents the median value of i^{th} block B_i and calculated as follows

Step1: Sort the pixel values of i^{th} block B_i of the given image I.

Step2: After sorting the pixel values in the block B_i, the CTV calculated using the median Med_i *is* given in Eq.6.

$$Med_i = \begin{Bmatrix} \frac{1}{2}\left(P_i^{\frac{n}{2}} + P_i^{\frac{n}{2}+1}\right), & if\ n\ \%2 = 0 \\ \left(P_i^{\frac{n+1}{2}}\right), & if\ \ n\%2 \neq 0 \end{Bmatrix} \quad (6)$$

where $n = 1,2..no\ of\ pixels\ \ of\ i^{th}\ block\ B_i$. $\left(P_i^{\frac{n}{2}}\right)$ is $(\frac{n}{2})^{th}$ pixel value of i^{th} block B_i, $\left(P_i^{\frac{n}{2}+1}\right)$ is $(\frac{n}{2}+1)^{th}$ pixel value of i^{th} the block B_i and $\left(P_i^{\frac{n+1}{2}}\right)$ is $(\frac{n+1}{2})^{th}$ pixel value of i^{th} the block B_i and $i = 1,2...m, no\ of\ blocks$ of the image I.

The CTV calculated using mode $Mode_i$ represents the mode value of the i^{th} block B_i of the image I and given in Eq.7.

$$Mode_i = \text{Most frequently occurring pixel value } P_i \text{ in } i^{th} \text{ the block } B_i \text{ of the image } I \quad (7)$$

where $i = 1,2,3...m$ and m is a number of blocks of the image I. The whole image is now presented using superpixels of blocks estimated using CTV. These superpixels are segmented using spectral clustering. The details for the segmentation of superpixels are described in the next subsection.

4.2.2. Segmentation of superpixels

The spectral clustering is performed on the superpixels values of blocks of the image. The segmentation of superpixels is performed to obtain tumour superpixels and non-tumour superpixels. The result of segmentation of superpixels is given in Fig 3 (c-d). The black colour specifies non-tumour superpixels and the white colour point represent tumour superpixels.

4.2.3. Identification of tumour block

The block of the image to which a tumour superpixel belongs to is identified in the original image. Since a tumour can extend across the tumour block, the adjacent blocks that have features similar to

tumour block are chosen from the original image to represent ROI. The Local Binary Pattern (LBP) based feature extraction technique is employed for recognition of adjacent blocks that possess similar characteristics as the tumour block *(T)*.

4.2.4. Identification of adjacent blocks

LBP is a popular feature extraction technique (Ojala et al., 2002) which plays a vital role in various applications like texture classification, segmentation of image, phase recognition and retrieval of images. The LBP operator gives the local spatial relation between the pixel and neighbouring pixels. It also describes the gray tone contrast. In the LBP feature extraction technique, the image is divided into small equal sized cells. Every pixel in the cell has eight neighbour pixels. The center pixel value is compared with the eight neighbouring pixel values. The neighbour, whose pixel value is greater than center pixel values is labelled as 1, else labelled as 0. Lastly, for every pixel, the eight-bit binary value is received. The obtained binary values are converted to decimal value and stored in LBP mask. The binary value is transformed to the decimal value in Eq (8).

$$LBP_{s,r}(x,y) = \sum_{s=0}^{s-1} g(f(x,y) - f(x_p, y_p))^{2s} \tag{8}$$

where $LBP_{s,r}$ is s neighbors on a circle of radius $r for a pixel x, y$. $f(x,y)$ is the gray value of the symmetric neighborhood pixel and $f(x_p, y_p)$ represent the gray value of the center pixel. The function g(w) gives the thresholding function and shown in Eq.9.

$$g(w) = \begin{Bmatrix} 1, w >= 0 \\ 0, w < 0 \end{Bmatrix} \tag{9}$$

where $w = f(x,y) - f(x_p, y_p)$. Then, the histogram is computed over decimal values of the blocks. The histogram is optimally normalized. The histograms of the blocks are concatenated to represent the feature vector. In the proposed method, the LBP histogram of the tumour block and eight neighbour blocks of the tumour block are compared to form ROI. The tumour block (T) determined in the previous step is considered as the center block. The center block has eight neighbour blocks $N_1, N_2 ... N_8$. The similarity between the histogram of the tumour block*(T)* and the neighbouring blocks is determined using Bhattacharya similarity metric (Aherne et al., 1997) and specified in the following Eq.10.

$$BC(H(T), H(N_i)) = \sum H(T) * H(N_i) \tag{10}$$

Where $H(T)$ is the histogram of the tumour block T and $H(N_i)$ representing the histogram of the i^{th} neighbourhood block N, $i = 1,2....8$.

The large BC coefficient represents similar histograms and vice versa. If the regions are similar, then the new region is labeled as a Tumor region. The operation of adjacent or neighbor blocks identification is repeated until no similarity exists between adjacent blocks and tumour block. Lastly, an obtained region is labelled as ROI. The ROI is given in Fig. 3(e-f). The algorithm for identifying tumours region called ROI is given below.

Algorithm for identification of ROI

Input: Input an MRI tumour image

Output: ROI

Step 1: Perform partitioning of the image into equal sized n *blocks* $b_1, b_2 .. b_n$.

Step 2: Compute superpixel value S of each block using Central Tendency Value

$S_i = CTV_{(i)}$ Where $i = 1,2.....n$. *n is the number of blocks.*

CTV is Central Tendency Value of the block, calculated using Eq.5.Eq.6.and Eq.7.

Step 3: Perform spectral clustering on superpixels S_i *where* $i = 1,2.....no\ of$ *superpixels to get clusters (* c_1 *=Tumor superpixels (white colour) and* c_2 *= Non-Tumor superpixels(black colour)).*

Step 4: Find the corresponding block of tumour superpixels (c_1) *in the image and label the block as tumour block(T).*

Step 5. Find adjacent blocks similar to tumour block (T) using LBP feature extraction to form ROI.

The segmentation of tumour tissues from ROI is reported in the succeeding sections.

4.3. Segmentation of ROI

The spectral clustering is directly applied on ROI that increases the speed of processing and the accuracy of segmentation. All the pixel value in ROI are considered for similarity matrix construction for spectral clustering. Since the size of ROI is small, the large similarity matrix formation can be avoided. No approximation is performed on similarity matrix construction to avoid dense similarity matrix formation. This serves to extend the high-quality accuracy of spectral clustering in the segmentation of tumour. The result of segmentation of TC from ROI is given in Fig. 3(g-h).

5. Experimental results and discussion

For experimental evidence, images are taken from the BRATS 2012 challenge dataset (Multimodal BRATS, 2012). The dataset contains 80 patient images. The details of the dataset are presented in Table 1. The MATLAB15a version running under the Windows-8 operating system with Intel R-core (TM) i5-4500U CPU 2.30GHZ, and 8 GB of memory (RAM) is employed for implementing, the proposed system. The sensitivity, specificity and dice score are used to evaluate the performance of segmentation and are given in Eq. 11, Eq. 12 and Eq. 13. The pixel by pixel comparison is made between ground truth and the segmented region in the proposed method.

Table 1. Description of BRATS 2012 dataset

	Synthetic images	Real patient images
High grade	25	20
Low grade	25	10

$$Sensitivity = \frac{TP}{TP + FN} \quad (11)$$

$$Specificity = \frac{TN}{TN + FP} \quad (12)$$

$$Dice\ score = \frac{2(TP)}{FN + 2(TP) + FP} \quad (13)$$

Where TN is True Negative that counts the number of correctly segmented negative case pixels in the segmented region. TP is True Positive that counts the number of correctly segmented positive case pixels in the segmented region. FN is False Negative that counts the number of incorrectly segmented negative case pixels in the segmented region. FP is False Positive that counts the number of incorrect segmented positive case pixels in the segmented region.

In the proposed method, 3D images from the dataset are preprocessed for bias correction using 3D Slicer. The 3D bias corrected image is converted to 2D and resized to 256*256 gray level image. The 2D segmentation of each slice is performed individually on the selected slice, and they are overlapped to produce the final result. Nonetheless, the slice may contain edema, Tumor Core (TC), necrotic, White matter, Gray matter, Cerebrospinal fluid (CSF) as various levels of the abnormal brain. As ground truth is available for edema and TC in the given dataset itself, the proposed method identifies edema and TC of the brain. From the experimental analysis, it is observed that the edema is extracted well from FLAIR images, where TC is extracted from T1 contrast image. However, to segment tumour tissue, spectral clustering is performed by considering n=2, where n is the number of cluster for edema and TC. To compare the obtained segmentation result with the ground truth, the size of ground truth is taken down to ROI.

In the proposed method, each image is partitioned into various block sizes. For each block, the CTV namely mean median and mode values are computed to produce the set of superpixels, where these superpixels act as the source for identifying the tumour blocks that constitute ROI. The segmentation of edema from ROI for synthetic high-grade FLAIR images is used to measure the efficiency of CTV and the selection of optimal block size. When smaller block size such as 2, 3, 4, and 5 are considered, the number of superpixels is increased. Thus the computational burden is increased. When the block size of 8 is considered, the number of tumour and the non-tumour pixels included in the ROI is optimal. When the block size of 16 and 32 are chosen, the number of tumour and the non-tumour pixels included in the ROI have been more and do not fulfil the intent of the proposed method. Hence, the optimal solution is obtained for block size 8 for which the number of superpixels is 32. It is observed from Fig. 4.a, that the mean and median provide almost the same dice score value for all block sizes, compared to that of a mode for segmentation of ROI. In addition to this, the execution time of the proposed work per image with regard to various block size for

segmentation of ROI is shown in Fig. 4.b. The mean and median requires little lesser processing time compared to that of the mode. The labelled tumour pixels can be useable in a block having non-tumour superpixel value in some instances. Those tumour pixels are available side by side to any of the segmented superpixel (segmented) block. Such tumour pixel blocks are identified by finding the adjacent blocks similar to tumour superpixel block using LBP feature extraction techniques for extracting ROI. The proposed method can also apply to tumour images were grade is not known to extract brain tumour tissues.

For diagnosing the MRI images using NLM filter, the parameters such as the ratio of search is set to 5, the ratio of similarity window is set to 2 and sigma (degree of filtering) is set as 3 experimentally. In the proposed work for segmenting ROI using spectral clustering, the k-nearest neighbors are set as 20 for the similarity matrix construction, and the sigma is set to 0.5 for Gaussian similarity distance metric.

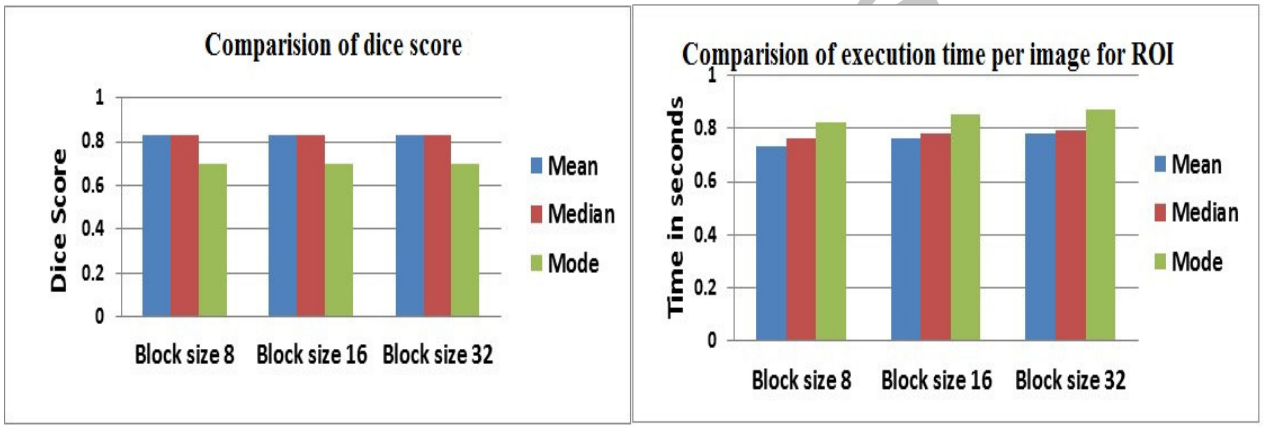

a **b**

Fig. 4. Comparison of proposed method for different block sizes and CTV values. a. Comparison of dice score values for segmentation of ROI. b. Comparison of execution time per image for segmentation of ROI.

The normalized Laplacian matrix is applied in the proposed method and the eigenvectors of Laplacian matrix are clustered using K means ++. This algorithm is employed for the cluster centroid specification. In this algorithm, initially, cluster centers are selected arbitrarily. The subsequent centers are selected based on the closest point's probability, relative to the squared distance from the existing cluster. The method is executed by 10 times as K means ++ is also not deterministic. Among 10 results obtained, the result with best objective function is required for clustering.

The KASP (Donghui et al., 2009) and Nystrom method (Fowlkes et al., 2004) are utilized for comparison of accuracy in the proposed method. The aim of KASP, Nystrom and the proposed method is to cut down the computation burden of dense similarity construction of spectral clustering. In the case of segmentation using Nystrom method, the original similarity matrix is not generated for spectral clustering as they randomly select pixel points from the given original matrix. In case of KASP method, cluster centers of K-means clustering have used for the expression of the similarity matrix. Hence, both the methods approximate the original similarity matrix and the

Table 2. Comparison of the dice score values of the proposed method with spectral clustering based methods.

Methods	Synthetic images (dice score)				Real patient images (dice score)			
	High grade		Low grade		High grade		Low grade	
	Edema	TC	edema	TC	Edema	TC	edema	TC
Nystrom method. (Fowlkes.et.al 2004)	0.48	0.79	0.42	0.61	0.51	0.28	0.26	0.33
KASP(Donghui.et. al 2009)	0.58	0.80	0.55	0.69	0.56	0.32	0.27	0.35
Proposed	**0.87**	**0.92**	**0.76**	**0.86**	**0.72**	**0.58**	**0.35**	**0.58**

accuracy of segmentation for less computation burden. To compare the proposed method with KASP (Donghui et al. 2009) and Nystrom method (Fowlkes et al. 2004), the codes available in the website for KASP(Wen-Yen, 2011) Nystrom method (Michael, 2004) has been reused and tested for BRATS 2012 challenge dataset. The results of the comparison of the dice score of the proposed method with KASP and Nystrom methods are listed in Table 2 for synthetic images (high grade and low grade) and real patient images (high grade and low grade). The proposed method yields better dice scores in both events, as all pixels in the ROI are considered for the similarity matrix construction for block size 8. Also the Fig 5. and Fig 6., shows the comparison of sensitivity and specificity values of the proposed method with KASP and Nystrom method. The extraction of edema and the TC of the proposed method are depicted in Fig 7.

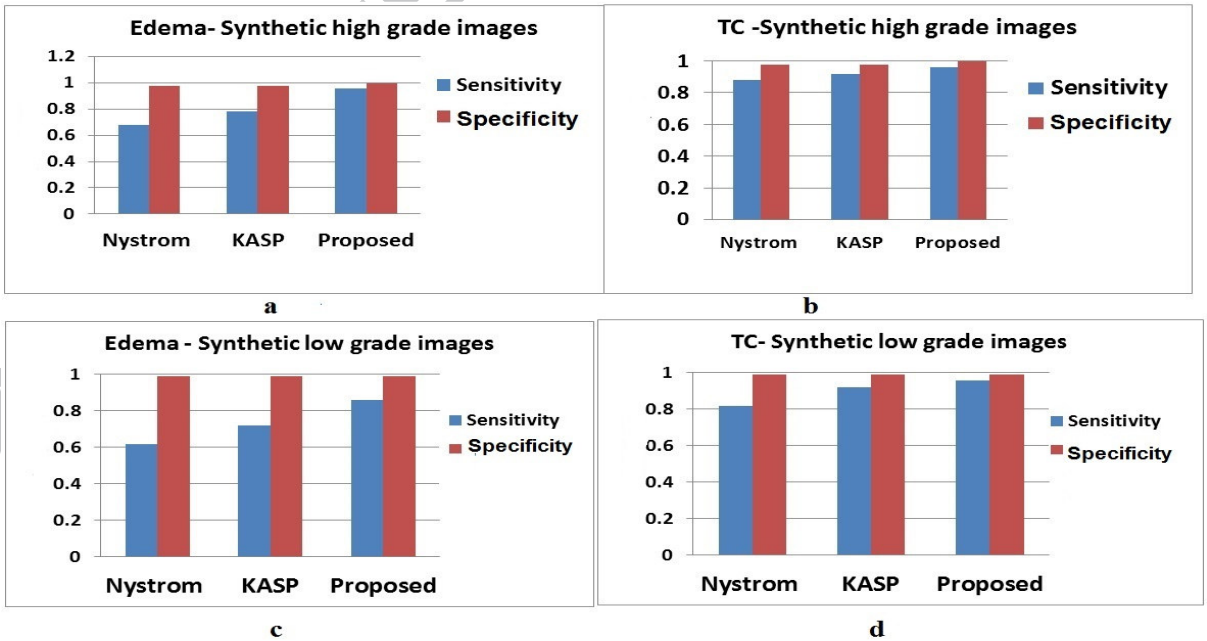

Fig 5. Comparison of sensitivity and specificity values of the proposed method with spectral clustering based methods for synthetic images. a. Edema – Synthetic high-grade images. b. TC -Synthetic high grade images. c. Edema - Synthetic low grade images. d. TC - Synthetic low grade images.

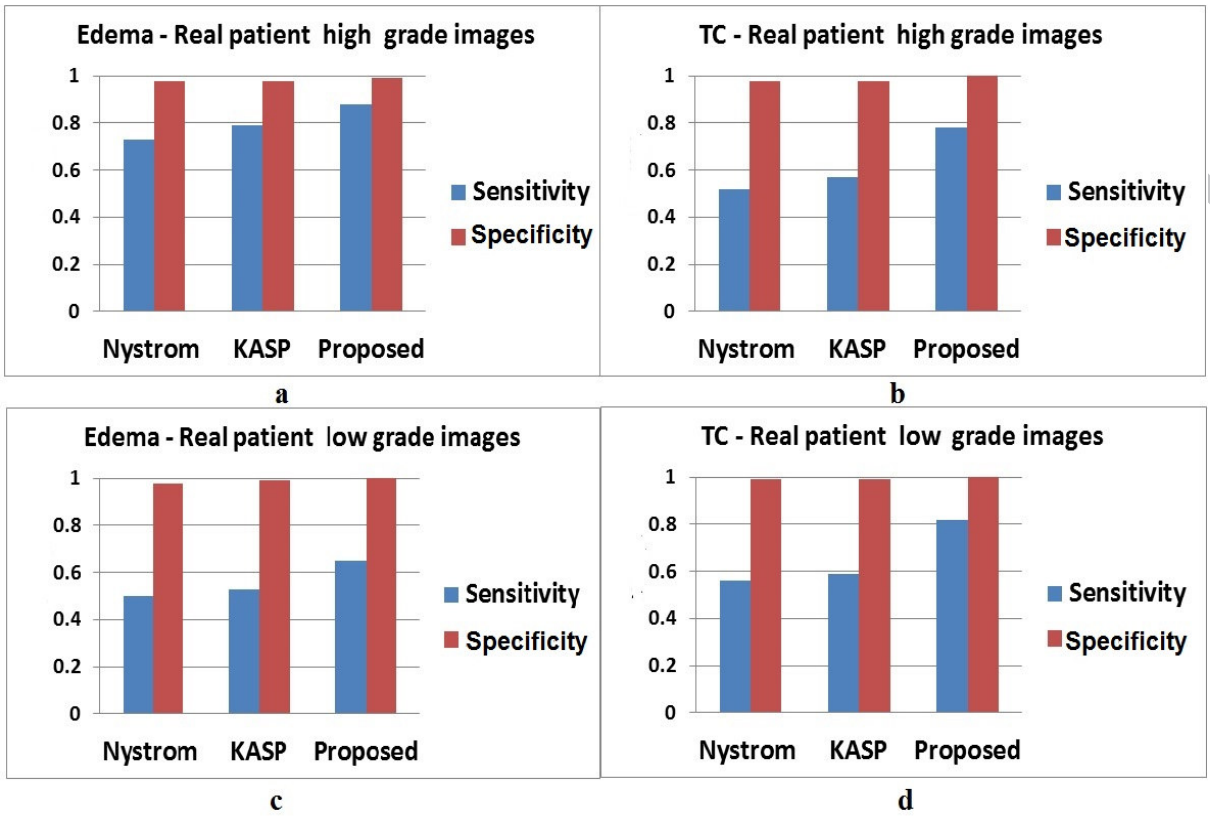

Fig 6. Comparison of sensitivity and specificity values of the proposed method with spectral clustering based methods for real patient images. a. Edema – Real patient high-grade images b. TC-Real patient high grade images. c. Edema - Real patient low grade images. TC – Real patient low grade images.

The comparison of the dice score values of the proposed method with other conventional clustering methods such as K-means, FCM and GMM for synthetic images and real patient images respectively are shown in Table 3. It is understood from Table 3, that the proposed method shows better dice score compared to the other clustering methods. This is because of the similarity matrix construction of SC, which is based on the distance metric, can quickly model the data with interpolation pattern and complex cluster configuration. The proposed method has produced better dice score than GMM for both real patient and synthetic images. As the complex pattern of a tumour has less intensity overlap and fewer artifacts in synthetic images, GMM is capable of producing dice score nearer to spectral clustering for synthetic images in the BRATS 2012 dataset. As GMM makes the solid assumption of Gaussian within-class data distribution cannot cope up with the example of complex cluster configuration with high-intensity overlap found in real images. So it produces less dice score for real patient images when compared with proposed method. The K-means algorithm and FCM produced less dice score due to its non-deterministic nature. The comparison of sensitivity and specificity values of the proposed method with K-means, FCM and GMM are presented in Fig 8 and Fig 9 for synthetic and real images respectively.

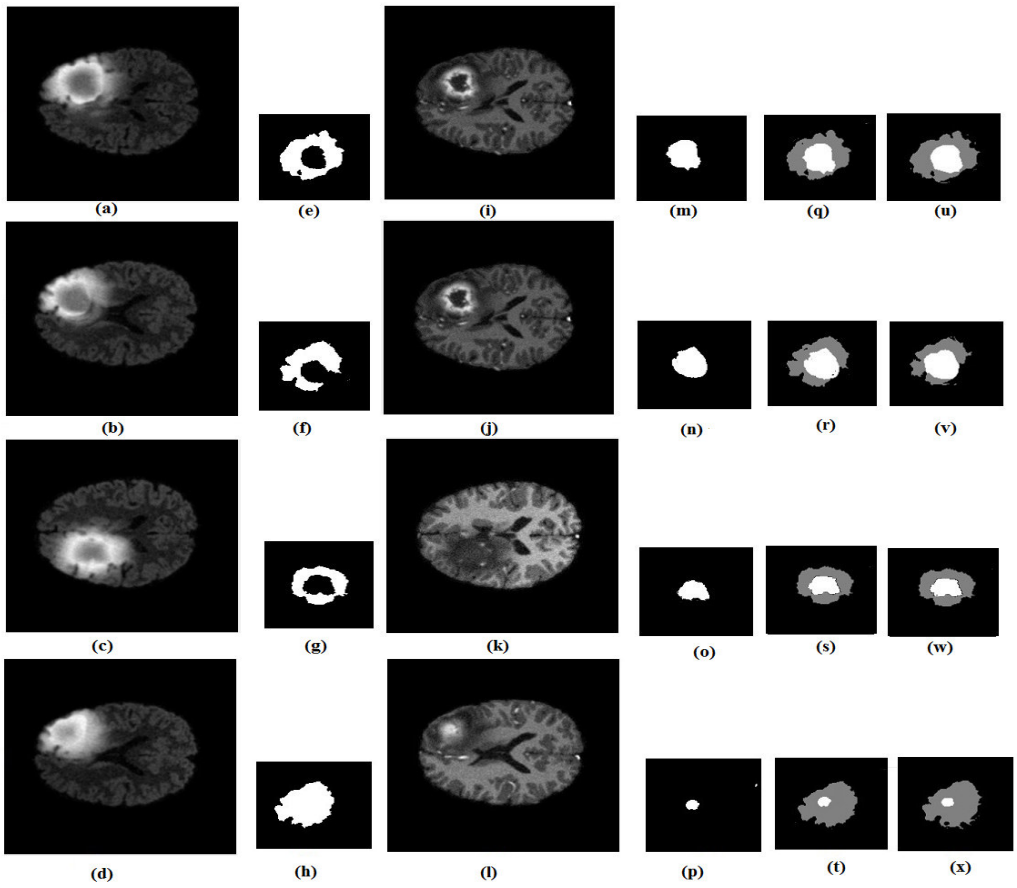

Fig. 7. Segmentation results of the proposed method for four patient images (FLAIR images (a)-(d) and T1 contrast images (i)-(l)). (e)-(h): Segmentation of edema (white colour) from ROI of FLAIR images. (m)-(p): Segmentation of TC(white colour) from ROI of T1 contrast images. (q) -(t): Overlap of edema (gray) and TC (white colour) as the final output images. (u) -(x): Ground truth images (reduced to the size of ROI).

Table 3. Comparison of dice score values of proposed method with conventional clustering methods

Methods	Synthetic images(dice score)				Real patient images (dice score)			
	High Grade		Low Grade		High Grade		Low Grade	
	edema	TC	edema	TC	edema	TC	edema	TC
Kmeans	0.72	0.64	0.51	0.60	0.55	0.21	0.19	0.22
FCM	0.76	0.82	0.74	0.78	0.61	0.29	0.23	0.25
GMM	0.83	0.86	0.71	0.82	0.69	0.30	0.25	0.28
Proposed	**0.87**	**0.92**	**0.76**	**0.86**	**0.72**	**0.58**	**0.35**	**0.58**

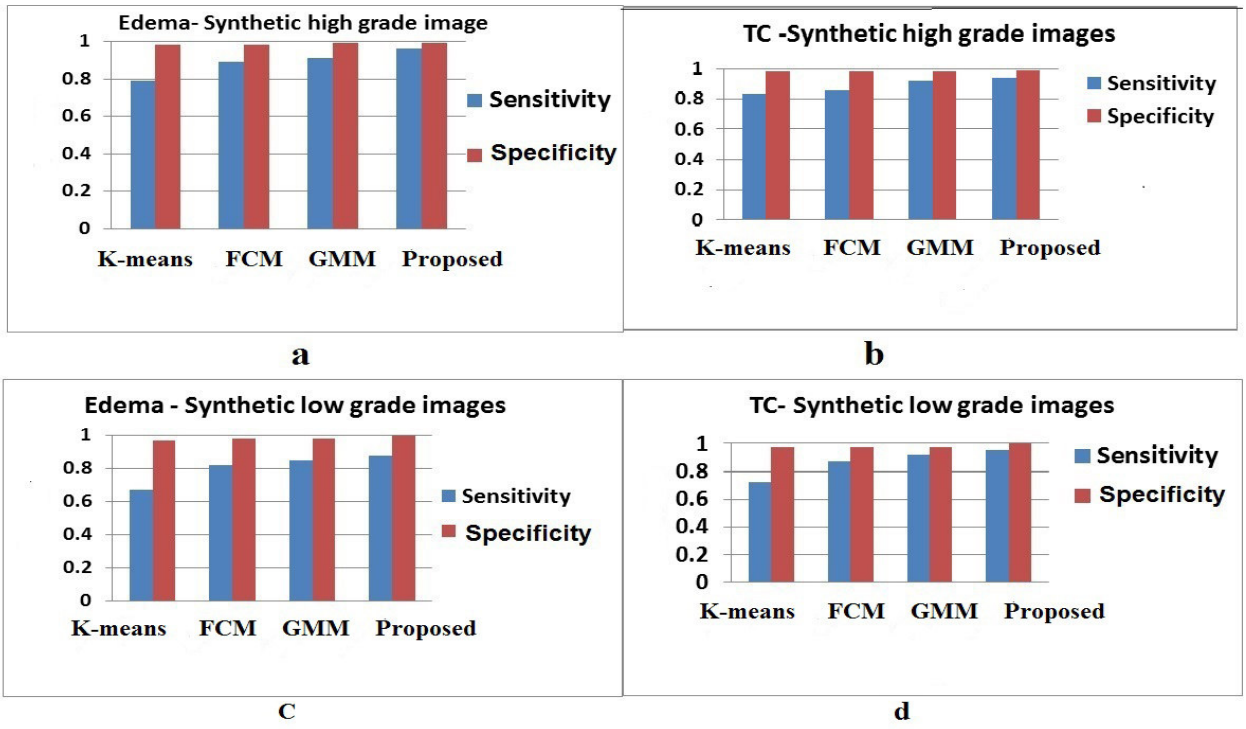

Fig. 8. Comparison of sensitivity and specificity values of proposed method with conventional clustering methods for synthetic images. a. Edema – Synthetic high grade images. b. TC - Synthetic high grade images. c. Edema - Synthetic low grade images. d. TC - Synthetic low grade images.

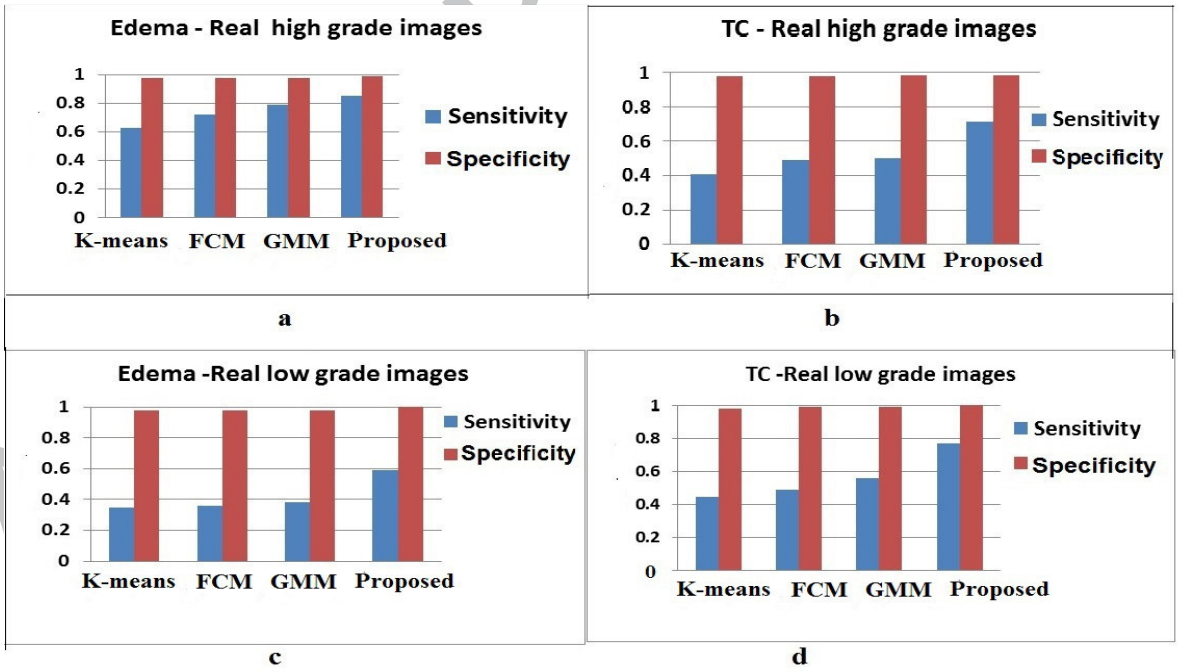

Fig. 9. Comparison of sensitivity and specificity values of proposed method with conventional clustering methods for real patient images. a Edema – Real patient high grade images. b. TC-Real patient high grade images. c. Edema - Real patient low grade images. TC – Real patient low grade images.

The comparision of dice score of the proposed work with Classification Forest (Darko et al., 2012) and Tumor-cut (Andac and Gozde, 2012) methods of BRATS 2012 challenge are shown in Table 4. The dice score values of these methods are taken from BRATS 2012 proceedings. The segmentation results of synthetic images and segmentation of edema of high-grade real images of proposed method are better compared to the other two methods. The low dice score is obtained for the low-grade real patient images as there was intense overlap between edema and the TC.

Table 4. Comparisons of dice score values of proposed method with BRATS 2012 challenge methods

Methods	Synthetic images(dice score)				Real patient images (dice score)			
	High grade		Low Grade		High Grade		Low Grade	
	edema	TC	edema	TC	edema	TC	edema	TC
Classification forest (Darko et.al ,2012)	0.65	0.90	0.55	0.71	0.70	0.71	**0.44**	0.62
Tumor cut (Andac and Gozde, 2012)	0.43	0.80	0.14	0.55	0.56	**0.73**	0.38	**0.71**
Proposed	**0.87**	**0.92**	**0.76**	**0.86**	**0.72**	0.58	0.35	0.58

In the paper (Darko.et.al, 2012), the authors have performed segmentation of a brain tumour as classification task using classification forest (CF). The inputs to classification forest are initial tissue probabilities, calculated using GMM and non-local context-sensitive features. The discriminative power of context-sensitive features, together with initial tissue probabilities as additional input increased the amount of context-sensitive information for the classifier. Thus obtained better dice score for critical cases (i.e.) for real patient images for (i) segmentation of edema and TC from low-grade real images and (ii) segmentation of TC from high-grade real images. However, the method takes more time for training the classifier when compared with the proposed method. In the paper (Andac and Gozde, 2012), the authors have performed multimodal brain tumour segmentation using Tumour–cut method. The multimodal image information increased the information for segmentation. Thus obtained better dice score for critical cases (i.e.) for real patient images. As proposed method used only region- level homogeneous cues (superpixels) as input to spectral clustering, we obtained less dice score for (i) segmentation of edema and TC from low-grade real images and (ii) segmentation of the TC of high-grade real images. Moreover, real patient images have high-intensity overlap. Therefore, multiple features must be extracted from the image to gain the better result. In future, to obtain better dice score , features such as texture and edge features can be integrated for segmentation of tumour using spectral clustering. Thus, the additional information in the image will increase segmentation accuracy.

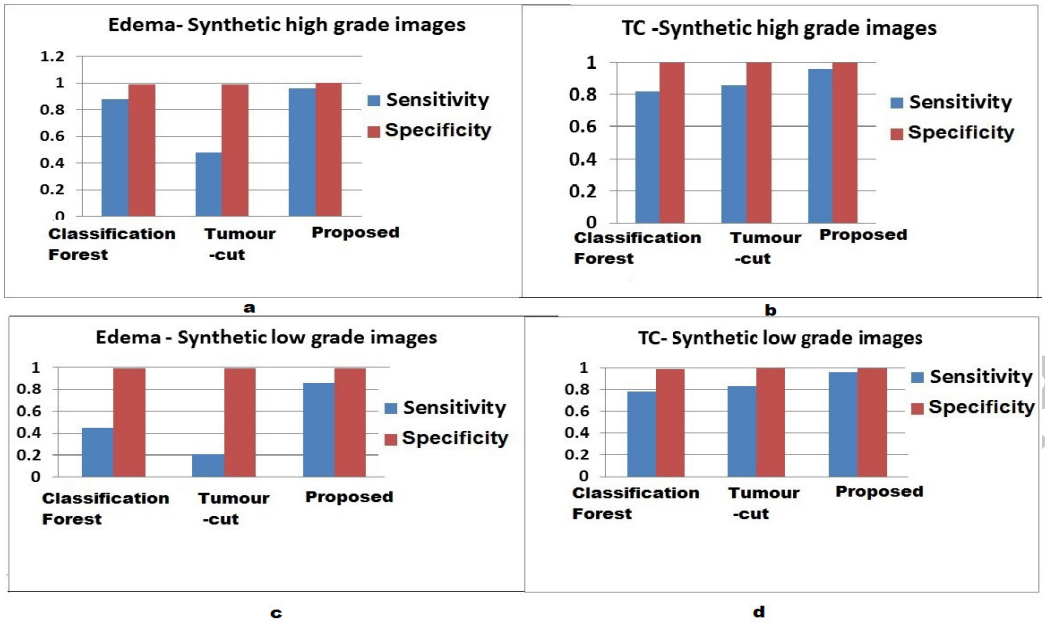

Fig. 10. Comparison of sensitivity and specificity value of proposed method with BRATS 2012 challenge methods for synthetic images. a. Edema – Synthetic high grade images. b. TC - Synthetic high grade images. c. Edema - Synthetic low grade images. d. TC - Synthetic low grade images.

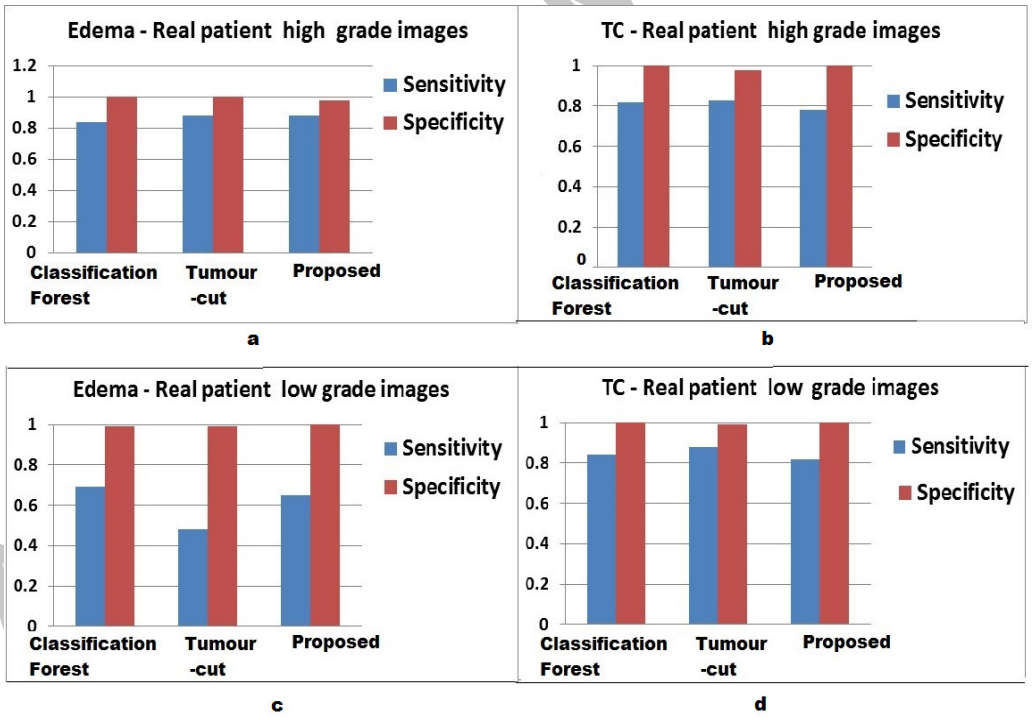

Fig. 11. Comparison of sensitivity and specificity value of proposed method with BRATS 2012 challenge methods for real patient images. a. Edema – Real patient high grade images b. TC-Real patient high grade images. c. Edema - Real patient low grade images. TC – Real patient low grade images.

The comparison of sensitivity and specificity value of the proposed method with BRATS 2012 challenge methods (taken from BRATS 2012 proceedings) are presented in Fig 10 and Fig 11 for synthetic and real images respectively.

Table 5. Overall execution time per patient in seconds for BRATS 2012 dataset

Methods	Time in seconds
Nystrom	24
KASP	26
K-Means	12
FCM	31
GMM	45
Proposed method	20

The execution time for BRATS 2012 dataset for the Nystrom, KASP, K-means, FCM, GMM and proposed method are given in Table 5. The execution time includes preprocessing time and the segmentation time for tumour tissues from T1 contrast image and FLAIR image of a single patient. These methods are evaluated on same set of images and run on same platform. The execution time of Classification Forest (Darko et.al, 2012) and Tumour-cut (Andac and Gozde, 2012) methods are not considered as they run on different platforms. From the Table 5, it is observed that K-means runs faster compared to other methods. Yet, it brings forth non -deterministic results and hard to get good clusters. The execution time of the proposed method is less compared to other methods. However, more focus will be made in future to obtain high dice score for real patient images.

6. Conclusion

In this paper, a method for automatic segmentation of brain tumour from the MRI images over ROI is proposed. The ROI (tumorous region) is identified using the superpixels based spectral clustering on the image. The superpixels are computed using the central tendency values of blocks of the image. Lastly, the ROI is segmented using the spectral clustering to segment tumour tissues. The dense similarity matrix construction is limited to the size of ROI for the spectral clustering, which in turn sustains the high-quality spectral clustering accuracy. The proposed method is used to segment tumour from the MRI images with the dice score of 0.8 and 0.9 for edema and TC respectively, for the high-grade synthetic images and dice score of 0.7 and 0.8 for edema and TC respectively for the low-grade synthetic images. In case of real patient images, the proposed method archives dice score of 0.7, 0.5 for edema and TC respectively for high grade images and dice score of 0.3, 0.5 for edema and TC respectively for low grade images. Our future work will focus on extracting multiple features from ROI for increasing segmentation accuracy.

References

Aherne,F., Thacker, N., Rockett, P., 1997. The Bhattacharyya Metric as an Absolute Similarity Measure for Frequency Coded Data. Kybernetika. 32(4), 1–7.

Andac, H., Gozde, U., 2012. Multimodal Brain Tumor Segmentation Using the "Tumor-cut" Method on The BRATS Dataset. Proceedings of MICCAI-BRATS Workshop. 19-22.

Andrew,Y.N., Jordan, M., Yier, W., 2001. On spectral clustering: analysis and an algorithm. Adv Neur In. 2, 849 – 856.

Angulakshmi,M., Lakshmi priya, G.G. 2017. Automated Brain Tumor Segmentation Techniques—A Review.International Journal of Imaging System and Technology. 27, 66–77.

Anitha Vishnuvarthanan, M., Pallikonda, R., Vishnuvarthanan, G., Yudong, Z., Arunprasanth, T., 2017. An automated hybrid approach using clustering and nature inspired optimization technique for improved tumor and tissue segmentation in magnetic resonance brain images. Applied Soft Computing. 57, 399-426.

Bauer, S., Wiest, R., Nolte, L.P., Reyes M., 2013. A survey of MRI based medical image analysis for brain tumor studies. Phys Med Biol. 58 (13), 97-129.

Buades, A., Coll, B., Morel, JM., 2005. A review of image denoising algorithms with a new one. Multiscale Model & Simulation. 4, 490–530.

Corso, J J., Sharon, E., Dube, S., El-Saden, S., Sinha, U., Yuille, A., 2008. Efficient multilevel brain tumor segmentation with integrated Bayesian model classification. IEEE Trans Med Imaging. 27(5), 629–640.

Darko, Z., Ben Glocker, E., Konukoglu, J.S., Antonio Criminisi, D. H. Ye, C. Demiralp, O. M. Thomas, T. Das, R. Jena, S. J. Price, 2012. Context-sensitive Classification Forests for Segmentation of Brain Tumor Tissues. Proceedings of MICCAI-BRATS workshop. 5-9.

Donghui, Y., Ling, H., Michael, I.J., 2009. Fast approximate spectral clustering.Proceedings of the 15th ACM SIGKDD international conference on Knowledge discovery and data mining. 907-916.

Emblem, K E., Nedregaard, B., Hald, J. K., Nome, T., Due-Tonnessen, P., Bjornerud, A., 2009. Automatic glioma characterization from dynamic susceptibility contrast imaging: brain tumor segmentation using knowledge-based fuzzy clustering.J Magn Reson Imaging. 30(1), 1-10.

Fowlkes,C., Belongie, S., Chung, F., Maik, J., 2004. Spectral clustering using the Nystrom method. IEEE T 1Pattern Anal. 26(2), 214–225.

GeethuMohan, M., MonicaSubashini, M., 2018. MRI based medical image analysis: Survey on brain tumor grade classification. Biomedical Signal Processing and Control. 38, 139-161.

Gordillo, N., Montseny, E., Sobrevilla, P., 2013.State of the art survey on MRI brain tumor segmentation. Magn. Reson. Imaging. 8, 1426–1438.

Jeetashree, A., PradiptaKumar, N., Niva, D., 2016. Modified possibilistic fuzzy C-means algorithms for segmentation of magnetic resonance image. Applied Soft Computing. 41, 104-119.

Jianbo, S., Jitendra, M., 2000. Normalized cuts and image segmentation. IEEE T Pattern Anal. 22(8), 888–905.

Juan-Albarracín, J., Fuster-Garcia,E., Manjón,J.V., Robles,M., Aparici,F., Martí-Bonmatí,L., García-Gomez.J.M., 2016. Automated glioblastoma segmentation based on a multiparametric structured unsupervised classification. PloS One, 10(5).

Liang, Z. , Wei, W., Jason, J.C., 2012. Brain tumor segmentation based on GMM and active contour method with a model-aware edge map. Proceedings of MICCAI-BRATS 2012. 24-2.

Madhukumar, S., Santhiyakumari , N., 2015. Evaluation of k-Means and fuzzy C-means segmentation on MR images of the brain. The Egyptian Journal of Radiology and Nuclear Medicine. 46, 475-479.

Menze, B., Reyes, M., Van L.K. et al., 2015. The multimodal brain tumor image segmentation benchmark (BRATS). IEEE Trans. Med. Imaging. 34(10), 1993–2024.

Michael, I.J., 2004. Fast approximate spectral clustering. http://www.cs.berkeley.edu/~jordan/fasp.html. (Accessed on 11 August 2016).

Multimodal brain tumor segmentation challenge (BRATS) 2012 dataset. http://www2.imm.dtu.dk/projects/BRATS2012. (Accessed 4 September 2016).

Ojala, T., Pietikainen, M., Maeenpaa, T., 2002. Multiresolution gray-scale and rotation invariant texture classification with local binary patterns. IEEE Transactions on Pattern Analysis and Machine Intelligence. 24, 971-987.

Padole, VB., Chaudhari, D., 2012. Detection of the brain tumor in MRI images using mean shift algorithm and normalized cut method. Int. J. Eng. Adv. Technol.1,53-56.

Phillips,W., Velthuizen, R., Phuphanich, S., Hall, L., Clarke, L., Silbiger, M., 1995. Application of fuzzy c-means segmentation technique for tissue differentiation in MR images of a hemorrhagic glioblastoma multiforme. Magn. Reson.Imaging. 13(2), 277–290.

Po, S., Jianhua, Y., Hai, L., Linda, C., Zhong, X., Stephen, T.W., 2013.Super pixel-based segmentation of glioblastoma multiform from multimodal MR images. Multimodal Brain Image Anal Lect Notes Comput Sci. 74–83.

Sauwen, N., Acou, M., Van, C.S., Sima, D. M., Veraart, J., Maes, F., Himmelreich, U., Achten, E., Van, H.S., 2016. Comparison of unsupervised classification methods for brain tumor segmentation using multi-parametric MRI. NeuroImage: Clinical.12, 753–764.

Tuhin, U. P, Samir, K. B., 2012. Segmentation of Brain Tumor from Brain MRI Images. Reintroducing K–Means with advanced Dual Localization Method. International Journal of Engineering Research and Applications. 2 (3), 226 – 231.

Tustison, N J, Avants, B.B, Cook, P., Zheng, Y., Egan, A., Yushkevich, P A., et al. 2010. N4ITK: Improved N3 bias Correction. IEEE Transactions on Medical Imaging. 29, 1310–1320.

Wen-Yen, C., 2014. Parallel Spectral Clustering in Distributed Systems. (Accessed 21 September 2016), http://alumni.cs.ucsb.edu/~wychen/sc.html.

Xiaofei, S., Lin, S., Yishan, L., Wei, Y., Hongpeng, L., Peipeng, L., Kuncheng, L., Vincent, C. T.M., Winnie, C. W. C., Defeng, W., 2015. Histogram-based normalization technique on human brain magnetic resonance images from different acquisitions. Biomed Eng Online,14.

Xiaofeng,R., Jitendra, M., 2003. Learning a classification model for segmentation. Proceedings of IEEE International Computer Vision Conference (ICCV). 10–17.

Yang, F., Grigsby, P. 2010. Spectral clustering for FDG-PET cervical tumor segmentation. Int. J. Radiat. Oncol. Biol. Phys. 78(3).

Yogita, K. D., Miind, M.M., Kajal, M., 2017.Segmentation of brain MR images using rough set based intuitionistic fuzzy clustering. Biocybernetics and Biomedical Engineering. 36, 413-426.

Yuhong, Li.,Faking, J., Jing, Q., 2016. Brain tumor segmentation from multimodal magnetic resonance images via sparse representation. Artificial Intelligence in Medicine. 73, 1-13.

Zexuan, J., Yong, X., Qiang, C., Quansen, S., Deshen, X., David, D.F., 2012. Fuzzy c-means clustering with weighted image patch for image segmentation, Applied Soft Computing.12, 1659–1667.

Captions for figures

Fig.1. a. FLAIR image b. T1 image c. T1 contrast image d. T2 image

Fig. 2. Flow diagram of the proposed work.

Fig. 3. Fig. 3. Segmentation result of the proposed method for two patient images (a) and (b). (a)-(b): T1 contrast brain tumour image. (c) -(d): Segmentation results of superpixels. (e)-(f) : ROI (g)-(h): TC

Fig. 4. Comparison of proposed method for different block sizes and CTV values. a. Comparison of dice score values for segmentation of ROI. b. Comparison of execution time per image for segmentation of ROI.

Fig 5. Comparison of sensitivity and specificity values of the proposed method with spectral clustering based methods for synthetic images. a. Edema – Synthetic high-grade images. b. TC -Synthetic low grade. c. Edema - Synthetic high-grade images. d. TC - Synthetic low-grade images.

Fig 6. Comparison of sensitivity and specificity values of the proposed method with spectral clustering based methods for real patient images a. Edema – Real patient high grade images b. TC-Real patient high grade images. c. Edema - Real patient low grade images. TC – Real patient low grade images.

Fig. 7. Segmentation results of the proposed method for four patient images (FLAIR images (a)-(d) and T1 contrast images(i)-(l)). (e)-(h): Segmentation of edema (white colour) from ROI of FLAIR images. (m)-(p): Segmentation of TC(white colour) from ROI of T1 contrast images. (q) -(t): Overlap of edema (gray) and TC (white colour) as the final output images. (u) -(x): Ground truth images (reduced to the size of ROI).

Fig 8. Comparison of sensitivity and specificity values of proposed method with conventional Clustering methods for synthetic images. a. Edema – Synthetic high-grade images. b. TC - Synthetic high grade images. c. Edema - Synthetic low grade images. d. TC - Synthetic low grade images

Fig. 9. Comparison of sensitivity and specificity values of the proposed method with conventional clustering methods for real patient images. a. Edema – Real patient high grade images. b. TC-Real patient high grade images. c. Edema - Real patient low grade images. TC – Real patient low grade images.

Fig. 10. Comparison of sensitivity and specificity values of proposed method with BRATS 2012 challenge methods for synthetic images. a. Edema – Synthetic high-grade images. b. TC -Synthetic high grade images. c. Edema - Synthetic low grade images. d. TC - Synthetic low grade images.

Fig. 11. Comparison of sensitivity and specificity values of proposed method with BRATS 2012 challenge methods for real patient images. a. Edema – Real patient high-grade images. b. TC-Real patient high grade images. c. Edema - Real patient low grade images. TC – Real patient low grade images.